ARMA 2881

Assessment of historic InSAR monitoring data prior to the Manefay Slide at the Bingham Canyon Mine using the latest analytical techniques

Williams C., Ross B.
Geotechnical Center of Excellence, University of Arizona, USA
Zebker M.
3vGeomatics Inc., Vancouver, Canada
Gaida M., Morkeh J.
Bingham Canyon Mine, Rio Tinto Kennecott Copper, Utah, USA
Robotham, M. E.
Rio Tinto Copper & Diamonds, Rio Tinto, Australia

ABSTRACT:

In April 2013, Rio Tinto Kennecott Copper's (RTKC) Bingham Canyon Mine experienced what is arguably the world's largest ever in-pit slope failure. The failure initiated on the East Wall, along a major, continuous, low-strength bedding fault, named the Manefay bed, and comprised approximately 145 million tonnes of rock and waste dump material. East wall slope deformations were detected some months prior to the catastrophic slope collapse by RTKC's ground based slope monitoring systems. Use of existing terrestrial radar and prism monitoring systems provided excellent data to manage the slope failure. The failure resulted in no injuries/loss of life, although the failure runout distance was larger than expected, resulting in the loss of mining equipment and significant production interruption.

Post failure investigations identified a RTKC sponsored, university research project which detected a zone of sporadic ground deformation at the crest of the Manefay failure using satellite based Interferometric Synthetic Aperture Radar (InSAR) data. When the outcomes of this research study were received in 2010, RTKC responded appropriately by conducting detailed field inspections and installing prisms in the area of concern.

Analytical methods for processing InSAR data have improved significantly since the time leading up to the Manefay failure. These updated methods have been used in this study of the available, historic InSAR data with results indicating that significant ground movements were occurring over a number of years prior to failure. Detailed knowledge of these movements could potentially have led to a different interpretation of failure mechanisms and magnitude and in hindsight, different slope management and mine development plans in the years preceding slope failure.

From a business and operations perspective, the ability to identify "weak signals" prior to catastrophic slope deformations is essential to appropriate management of such events. The use of InSAR, as discussed in this paper, provides an increased capability for further improved slope management at RTKC, and at other mining operations.

1. INTRODUCTION

On April 10th, 2013 the Manefay Failure (landslide) occurred at the Bingham Canyon Mine, just outside of Salt Lake City, Utah. The Manefay failure occurred in two events, the first event at 9:30 pm and the second event at 11:05pm (Pankow et al., 2013). In total, the slide mass comprised approximately 145 million tonnes of rock and waste dump material. The Manefay slope failure is arguably the largest in-pit landslide in the history of mining and is shown in Figure 1. Before and after views of the failure are shown in Figure 2.

The Manefay slide deformation was identified at the mine around the beginning of 2013. As the slope deformation continued, the timing of the slope failure was predicted, and the subsequent failure was managed with no injuries or loss of life.

While the timing of the event was well managed, the failure mechanism was not well understood. Subsequently, the failure mass and run-out distance were under predicted, resulting in a significant loss of equipment and impacts to mine production.

The failure developed in the upper northeast wall of the pit, which was a largely unconfined nose-shaped geometry (see Figure 2). The primary causal factor of failure was the presence, orientation and character of the Manefay bedding plane fault which formed the basal plane to this large complex wedge (Figure 1).

Over the nine years since failure, processing technologies for Interferometric Synthetic Aperture Radar (InSAR) data have advanced significantly. This study seeks to better understand whether these advances could have been used to detect "weak signals" prior to catastrophic damage from the April 2013 Manefay slope failure and how this could be applied in future at the Bingham Canyon Mine and across our industry.

2. BACKGROUND INFORMATION

In assessing the value of InSAR data relative to this failure, it is important to understand the following:

- The geology of the failure area;
- Ground based monitoring at the time of failure;
- The mechanism of failure; and,
- Interpretation of available InSAR data at the time of failure - 2010 InSAR research project.

2.1. Geology

Bingham Deposit and Regional Setting

The Bingham Canyon Mine represents a classic porphyry copper system which contains copper, gold, silver, molybdenum, lead, and zinc. Permian and Pennsylvanian sedimentary units were thrusted on multiple large faults, from the west to the east during the Sevier Orogeny (Presnell, 1997). The sediments stopped in their final location in the Oquirrh Mountain Range after colliding with the higher ground of the Uinta Arch. The region was then extended in the beginning of the Eocene Period/Era around 42 to 50 million years ago (Moffit, et al., 2018). Then, approximately 37 to 38 million years ago, a large monzonite intruded into the sediments (Porter et al, 2012). Subsequent intrusive events containing quartz monzonite porphyry, porphyritic quartz monzonite, latite porphyry, and finally quartz latite porphyry, enriched the mineralization of the deposit, making Bingham Canyon one of the world's largest copper deposits (Porter et al, 2012).

Figure 1: Aerial photograph of the Manefay Failure, looking north. Image captured 24 hours after the collapse

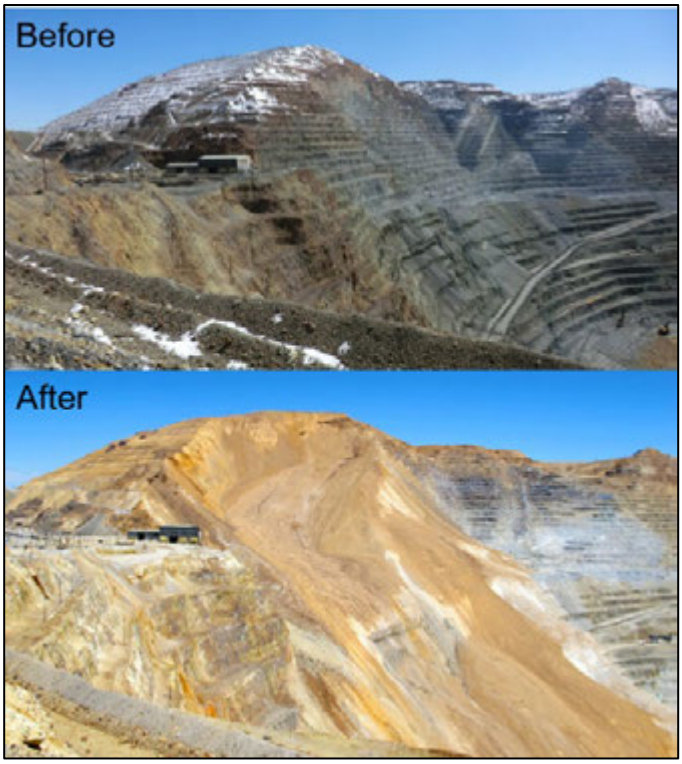

Figure 2: Before and after photographs of the Manefay Failure, looking northeast

Manefay Geology

The Manefay failure was made up of four material types:

- Calcareous Sandstone and Sandy Limestone beds, (altered to hornfels near the intrusion);
- Latite Porphyry Intrusion;
- Quartzite; and
- Mine Waste (Rail Dumps).

The Manefay bed comprises sandy limestone which was altered to hornfels and formed a weak bedding plane fault. This fault is believed to have been mobilized during the Sevier thrusting, the Eocene Basin and Range extension, and during the emplacement of the Bingham Stock. These events resulted in a weak, continuous, clay, fault gouge along the Manefay fault. The intrusion of a Latite Porphyry Sill, associated with the Starless Dike, further lowered the fault shear strength. The Manefay Failure mass is split by the Latite Porphyry Starless Dike. Quartzites stratigraphically overly the Manefay bed. The geology of the Manefay area is shown in Figure 3

The emplacement of the Bingham Stock caused folding of the Quartzites creating the Bingham Syncline to the North East of the intrusion. The Bingham Syncline is also shown in Figure 3.

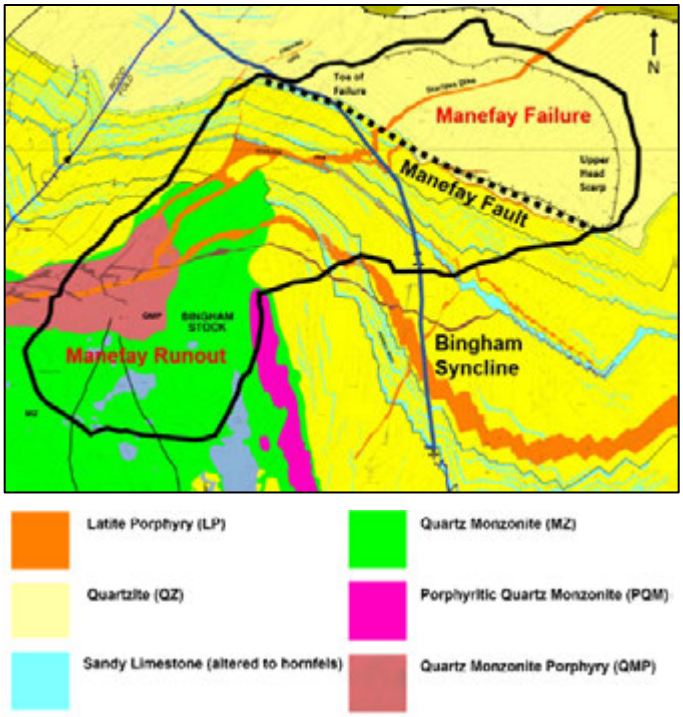

Figure 3: Geologic map of Manefay Area Post Failure, (adapted from Gibbs, 2018)

2.2. *Ground Based Monitoring*

In 2013, the systems that were in place for monitoring of the Manefay slope consisted of the following:

- Prisms measured by Robotic Total Stations (RTS);
- Synthetic Aperture Radar (SAR) ;
- Real Aperture Radar (RAR); and
- Wireline Extensometers.

In addition to the above, a system of annual slope hazard awareness training was delivered to all mine staff, to provide "trained eyes everywhere" in the pit to assist with slope monitoring and management efforts. In 2013, and even in 2019, these monitoring systems would be considered best practice for pit slope deformation monitoring.

The 2013 monitoring systems performed well prior to failure and provided multiple, independent sources of data which could be cross referenced and validated to allow accurate prediction of the timing of failure.

The RTS and Radar systems had limited ability to see beyond the crest of the pit due to line of sight and obliquity limitations from their established locations. This is illustrated in Figure 4, with the dark grey area being outside the view of the SAR. Some mobile monitoring was relocated to minimize coverage gaps when the Manefay instability was identified. The view from the Real Aperture Radar is shown in Figure 5. The RAR was able to see around the nose shape geometry of the slope. Although the area around the nose is oblique to the line of

sight of the radar for deformation magnitude, this location allowed identification of failure deformation limits. The areas beyond the crest of the mine were monitored with detailed, visual inspections, GPS surveys, and via annual airborne LiDAR surveys.

InSAR monitoring was added, to supplement ground-based monitoring systems, at RTKC in 2016.

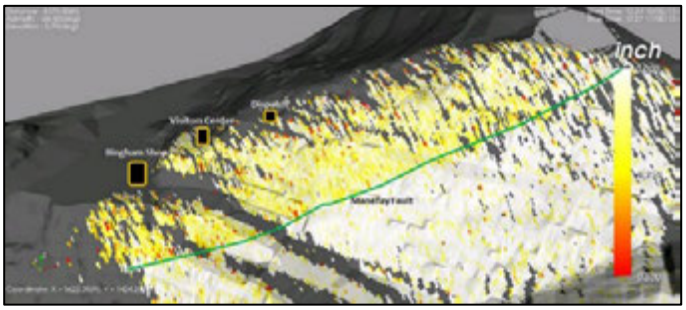

Figure 4: Example of a SAR scan area, February 2013

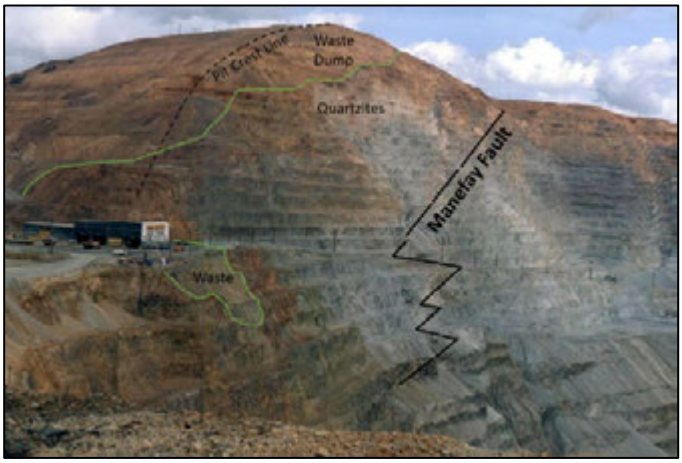

Figure 5: RAR view, with approximate trace of Manefay fault, February 2013

2.3. *Mechanism of failure*

The mechanism of the Manefay slide has been studied by numerous geotechnical experts. The consensus is that the mechanism was a complex, active/passive block failure, with the basal plane of the failure being along the Manefay bedding fault.

The orientation of the Manefay Bed is a product of the Bingham Syncline folding. The failure geometry essentially comprises an active upper block where the bed is dipping to the northwest, approximately parallel to the strike of the slope, and a lower passive block with shallower dips, trending westerly and into of the wall.

The upper margin of the Manefay failure slope comprised old waste dump materials which may have added load and potentially contributed to the instability. The relationship between rock and waste dump materials is shown in Figure 6.

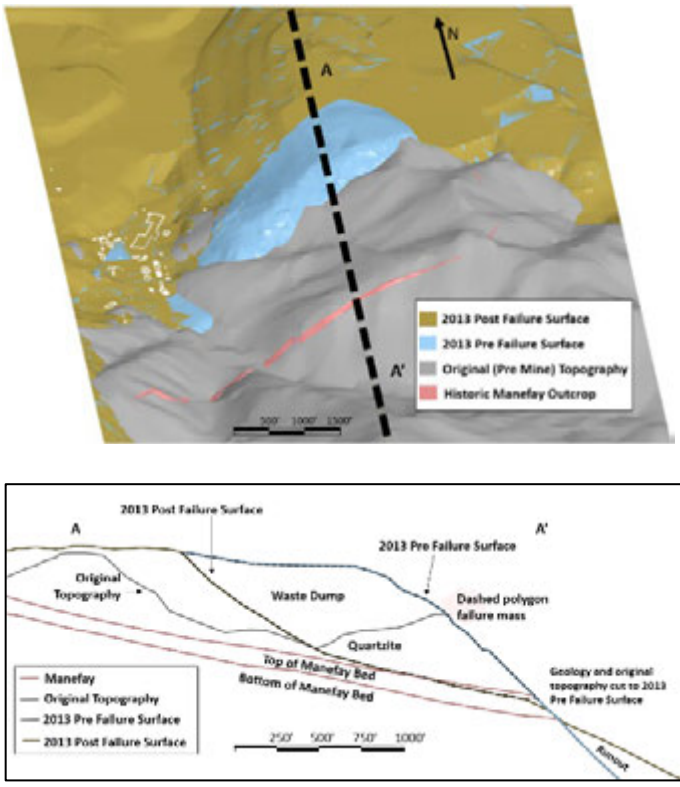

Figure 6: Schematic plan and cross section showing relation of the rock to waste dump in the upper section of the Manefay Failure, (Gibbs, 2019)

2.4. *2010 InSAR Research Project*

In 2010, a research study was completed integrating InSAR data with advanced 3D numerical modeling at Rio Tinto's Palabora and Bingham Canyon Mine Operations. This study was completed as part of the Mine Subsidence Monitoring (MSM) Project, which was a joint project undertaken by University of British Columbia and Simon Fraser University. During the InSAR evaluation of the Bingham Canyon Mine, a deforming mass was identified, in the upper area of what is now known as the Manefay slide. The area showed movement in the Manefay mass in 2008, and regression of movement in 2009 (Eberhardt, et al. 2010). The area was inspected in detail, and additional prisms were placed in the zone of concern immediately following receipt of this study.

3. OBJECTIVE OF STUDY

In 2018, Rio Tinto engaged 3vGeomatics Inc. to assess the available, historic InSAR data in the period leading up to the Manefay failure using the latest analytical techniques. This, in hindsight, could help better understand:

- Whether InSAR monitoring could have detected "weak signals" prior to the Manefay slope failure;
- Whether the extent of the movement behind the pit crest could have been better estimated;

- Our confidence in use of InSAR to support strategic slope risk management at RTKC and elsewhere across Rio Tinto; and
- The strengths and limitations of InSAR data analysis in comparison to ground based radar systems.

4. SCOPE OF STUDY

This study used satellite based InSAR data to detect and measure surface displacements from 2008 leading up to the Manefay Slide in 2013. The advantages of InSAR when compared to other ground-based monitoring systems include the ability to monitor large areas, availability of historical data, and up to 1-2 mm of precision, making it highly suitable for this analysis. This analysis technique produced a deformation time series using all available data, which was analyzed for trends leading up to the Manefay Slide.

5. SAR DATA

The satellite data used for this analysis was acquired by the Canadian RADARSAT-2 (RS2) satellite. RS2 is a C-band radar satellite with a resolution of 3m in ultra-fine mode. The ascending and descending image footprints of the Bingham Canyon Mine area are shown in Figure 7. A total of 22 ascending and 70 descending images were analyzed spanning 2008 to 2013.

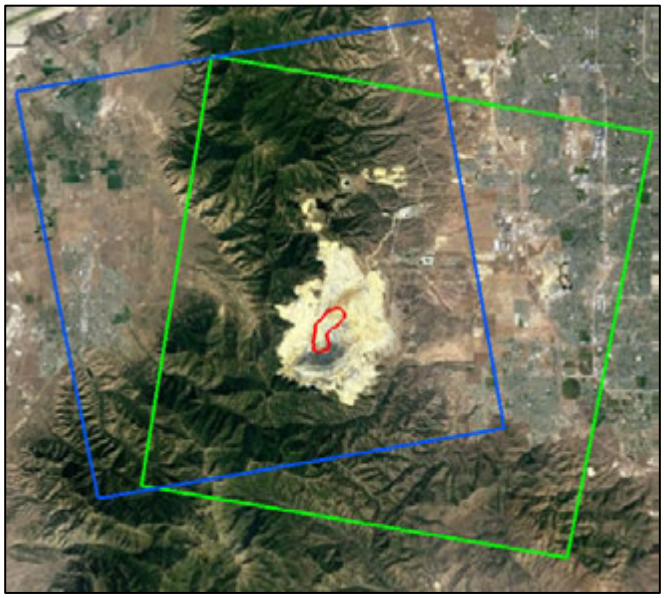

Figure 7: Ascending (blue) and descending (green) footprints of the RADARSAT-2 images and the Manefay Slide and run out area (red)

Because of the geometry of the pit slope and the viewing angle of the satellite pass, the descending data has better sensitivity to down slope displacement in the Manefay failure area and all available descending data was used from the launch of RS2 (in 2008) to June 2013 (after failure). The ascending images were used to allow for a dual pass analysis in which displacement direction can be resolved in a 2D plane. This is further discussed in Section 6.4.

6. ANALYTICAL METHODOLOGY FOR INSAR PROCESSING

The InSAR processing approach for this analysis, from initial data to deformation time series products consists of three general steps: stack pre-processing, signal enhancement, and phase unwrapping and parameter estimation (see Figure 8). These steps are discussed as follows:

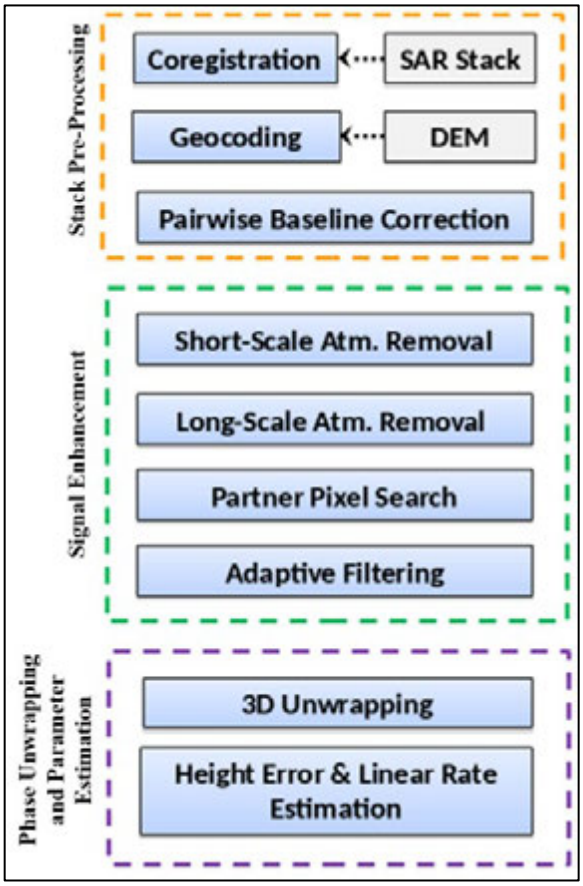

Figure 8: General InSAR processing chain used for this analysis.

6.1. SAR Pre-processing

Successive SAR images are co-registered with a chosen master scene to account for differences in satellite position. Interferograms are then generated from pairs of SAR images. These are the fundamental observable data for InSAR and contain the per-pixel, phase differences between images. This includes ground displacement. Typically, modern InSAR analyses, involve forming a network of many interferograms, connected by their

common dates. A Digital Elevation Model (DEM), is used to remove unwanted topographic signals in the interferograms.

6.2. *Signal Enhancement*

Prior to signal enhancement, the interferograms contain atmospheric effects, errors in the DEM, noise, and ground displacement. Hydrostatic and tropospheric atmospheric effects are then modeled and removed, after which, an adaptive filter is applied to enhance data and suppress noise. Figure 9 shows the successive stages of signal enhancement for an interferogram, with non-moving background areas re-referenced to zero radians.

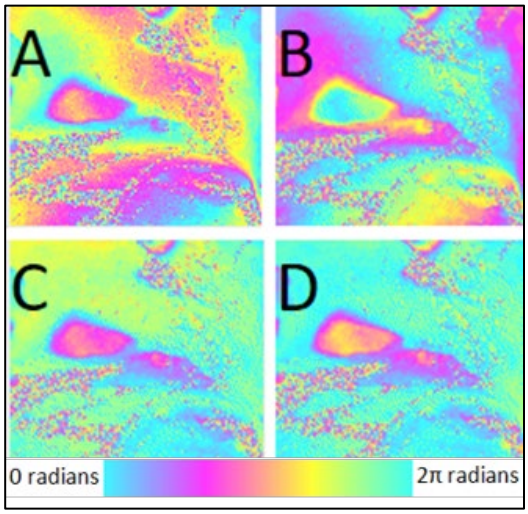

Figure 9: Signal enhancement process shown over the Manefay slide. Corrections to each interferogram include removing topography (A), orbit errors (B), hydrostatic atmosphere (C), and tropospheric atmosphere (D).

6.3. *Phase Unwrapping and Parameter Estimation*

Interferograms contain pixels with phase values between 0 and 2π radians; this is termed "wrapped" phase. Unwrapping attempts to integrate these values into an absolute "unwrapped" phase by analyzing how wrapped phase values change over space and time. This is challenging as naturally occurring discontinuities in the data are commonplace, such as very fast displacement areas, waterbodies, areas of disturbance between the two image dates and areas not covered by the viewing geometry.

A linear regression is used to jointly solve for displacement and DEM error from the network of unwrapped interferograms. Areas of noise are then masked from the data (Figure 10). These final stage interferograms contain ground displacement and some residual atmosphere.

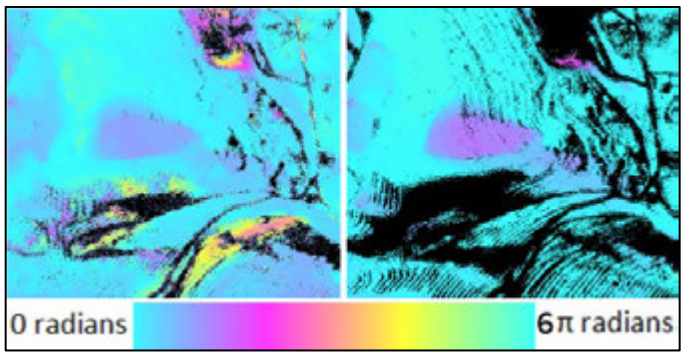

Figure 10: An unwrapped interferogram (left) and the same interferogram following DEM error correction and noise masking (right).

6.4. *Using InSAR Displacement Histories*

While line of sight (LOS) displacement time series can be resolved for a single stack of images, two independent stacks, one ascending and one descending, can be combined to produce a time series with displacement direction information. Displacement is calculated in the 2D, up-down, east-west plane. The direction of displacement can be computed for areas of displacement with overlapping coverage from the two stacks. Respective LOS displacement estimates from the two passes are then co-projected along this solved vector, changing the magnitude of displacement appropriately (Figure 11). Figure 12 shows the site with arrows to indicate the satellite headings and look directions for the two passes.

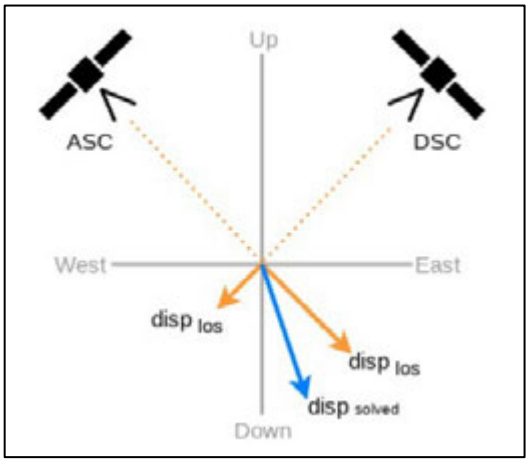

Figure 11: Two line of sight measurements can be combined to solve the direction of displacement in a 2D, east-west, up-down plane.

Figure 12: 3D View of the site with ascending and descending passes. Ascending orbit on the left, heading north and looking east; descending orbit on the right, heading south, looking west. The black polygon represents the Manefay Failure.

7. RESULTS OF STUDY

The results of the InSAR analysis were presented in multiple forms for assessment, as follows:

- Raster plots of deformation rates were examined on an annual basis and compared to geology;
- Time series of areas within and around the failure; and
- Directionality of movement.

7.1. Annual Raster Plots of Deformation Rate

Figures 13 to 17 show resolved deformation from the evaluation of both the ascending and descending InSAR data sets on an approximate annual basis (refer Section 6.4). The assessment indicates that deformation was evident in the approximate area of the Manefay Failure as far back as 2008.

The annual raster plots show that the shape of the failure was well developed in 2008 to 2009 and broadly matches the final extents of the failure. As in the MSM Project (Eberhardt et al., 2010), regressive movement is suggested between 2009 and 2010, and then progressive movement in 2010 to 2011. Increased "noise" in the period immediately prior to failure due to winter conditions, in addition to the high movement rates that resulted in phase ambiguity, made the final acceleration unclear in the last time step (see Figure 17).

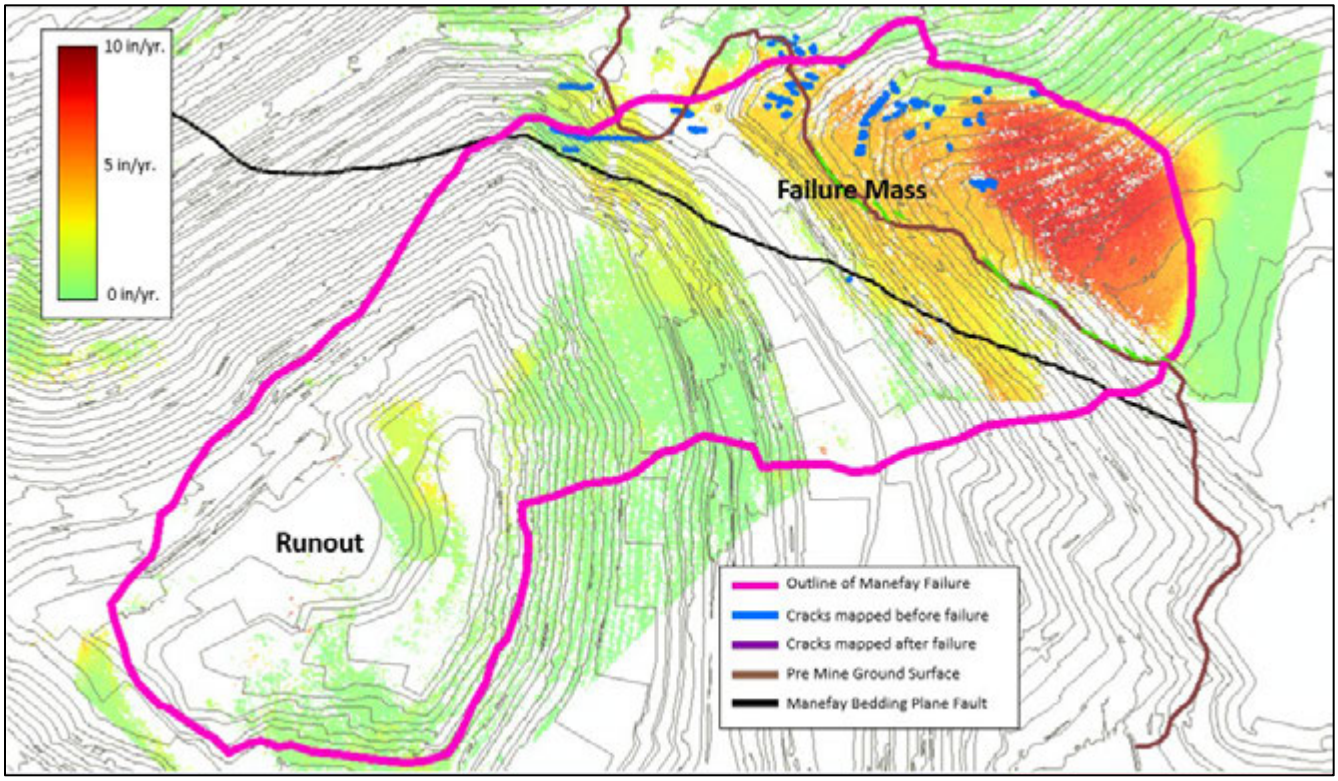

Figure 13: Resolved InSAR rate averaged from September 5th, 2008 to July 14th, 2009 (10 in/yr. velocity scale)

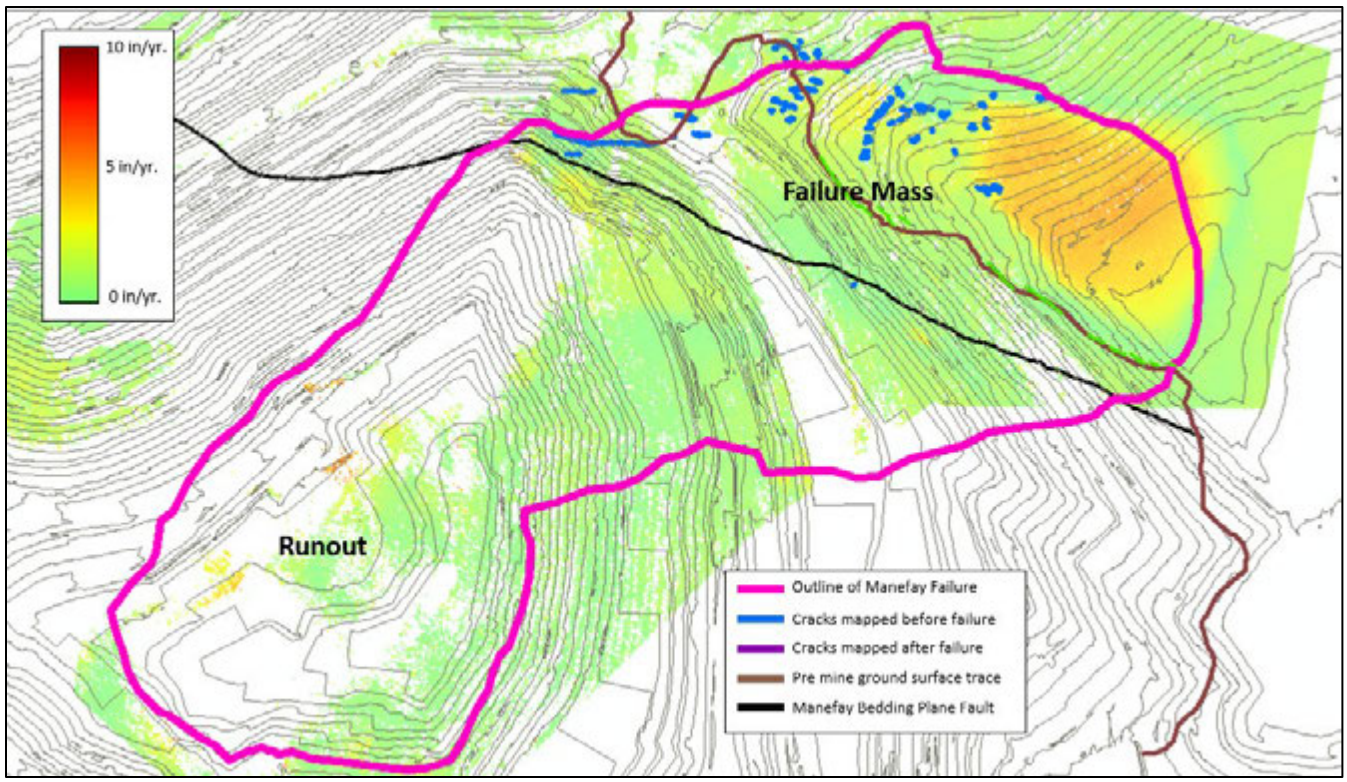

Figure 14: Resolved InSAR rate averaged from July 14th, 2009 to August 2nd, 2010 (10 in/yr. velocity scale)

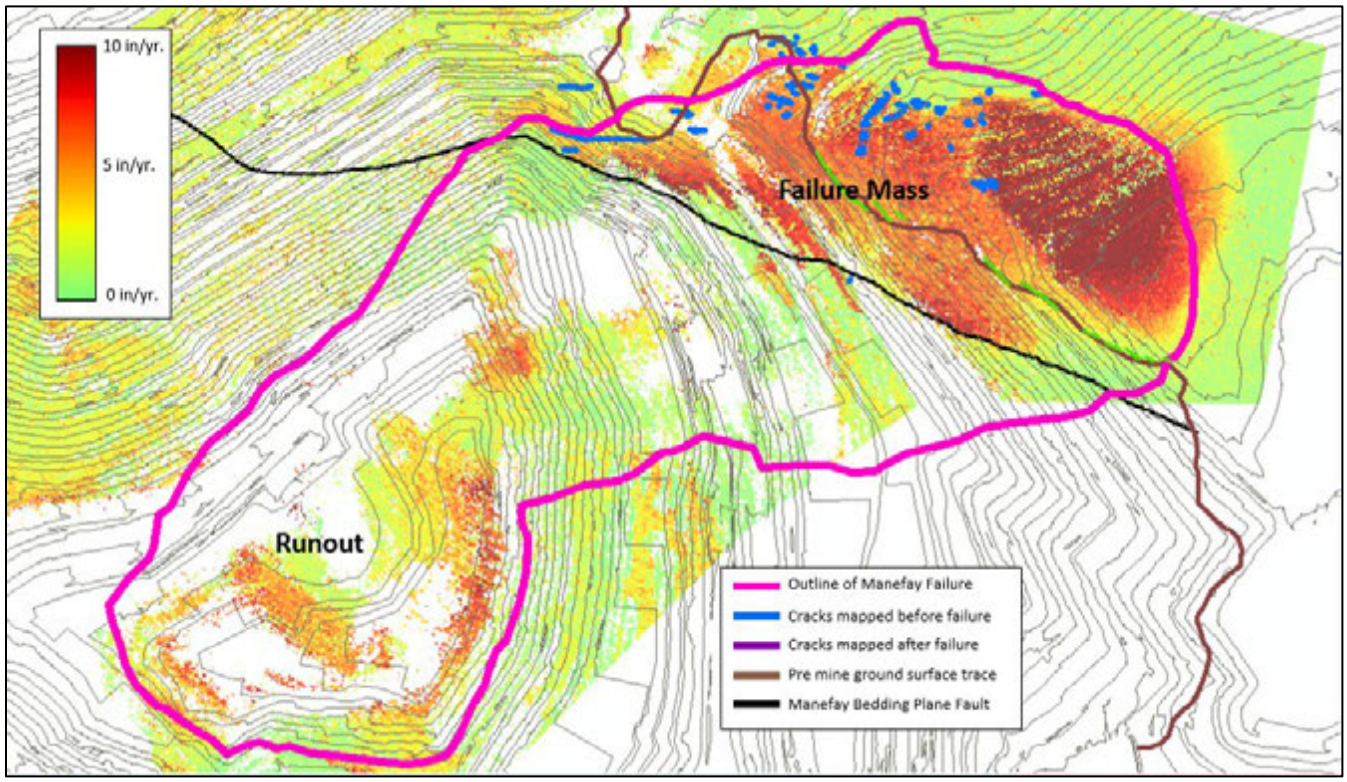

Figure 15: Resolved InSAR rate averaged from August 2nd, 2010 to July 4th, 2011 (10 in/yr. velocity scale)

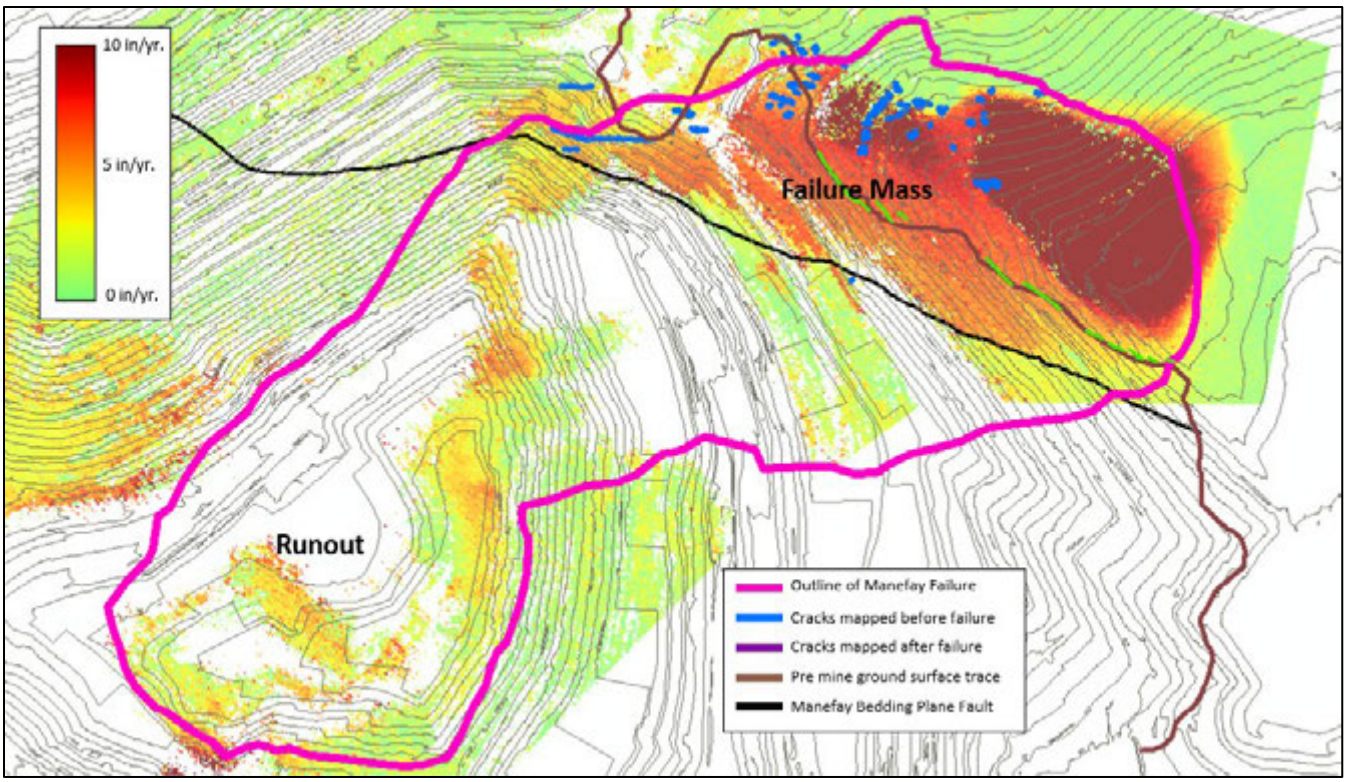

Figure 16: Resolved InSAR rate averaged from July 4th, 2011 to July 22nd, 2012 (10 in/yr. velocity scale)

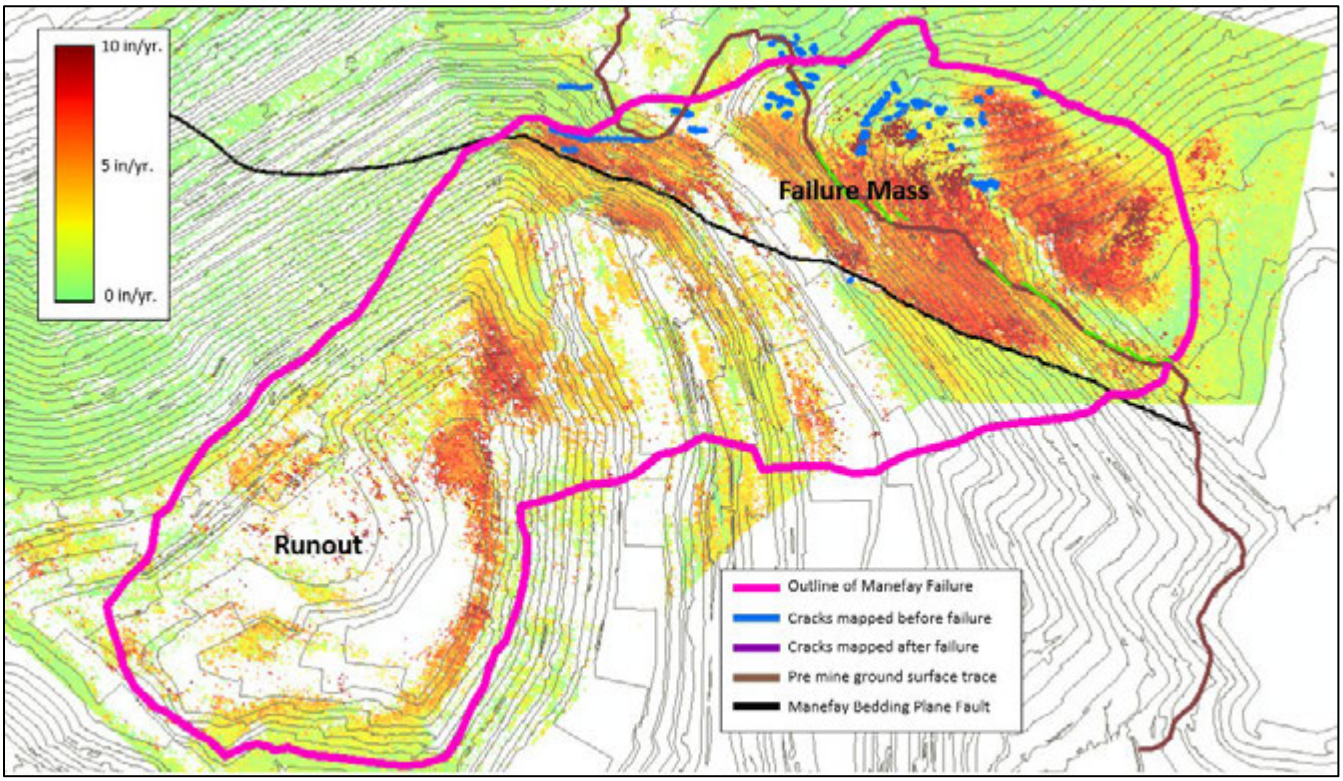

Figure 17: Resolved InSAR rate averaged from July 22nd, 2012 to March 3rd, 2013 (10 in/yr. velocity scale).

7.2. *Analysis of time series of regions inside and around the Manefay Slide*

Various regions of the slide were evaluated based on the deformation patterns observed in the annual rate raster plots and relative to known geologic features. The areas selected are shown in Figures 18 and 19 and are described as follows:

- G1 - Hotspot of deformation in the waste dump high on the slope. Slope is facing north west, and around the nose area;
- G2 - Waste dump slope facing southwest towards the pit;
- G3 - Rock slope facing the pit in the active block of the failure, stratigraphically above the Manefay Bed and below the waste dump;
- G4 - Approximate transition between active and passive block of the failure, below the waste dump contact area;
- G5 - Area in the passive block of the failure;
- G6 - Most western point of the passive block of the failure;
- G7 and G8 - Areas below the passive block of the failure, and stratigraphically below the Manefay bed showing deformation;
- G9 - Office level, which had cracking observed post failure; and
- G10 - Represents a known stable area on the West Wall and is shown in Figure 19.

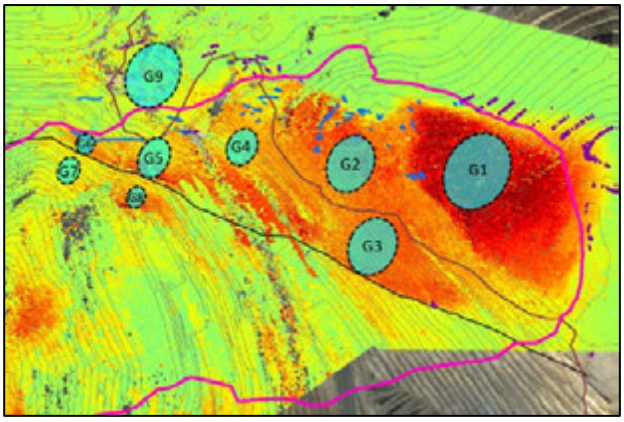

Figure 18: Areas assessed with deformation time series described above.

For the areas selected within the slide mass, a slight regressive trend is evident following the first data gap, in May of 2008 (see Figure 20). However, after the second data gap, in August of 2010, the trend turns progressive and accelerates through 2011.

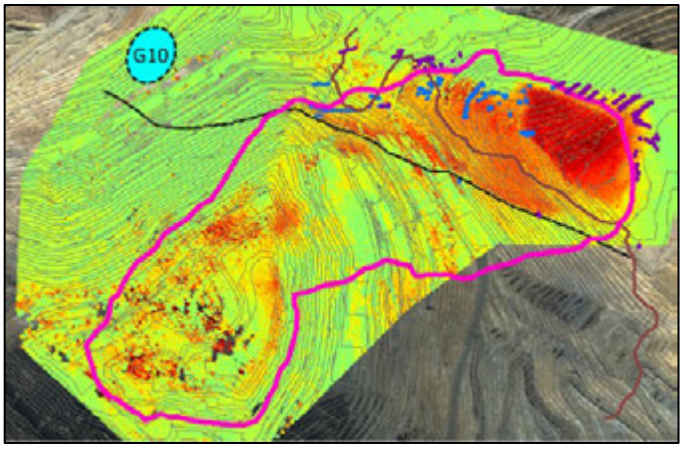

Figure 19: G10, stable comparison area, on the West Wall.

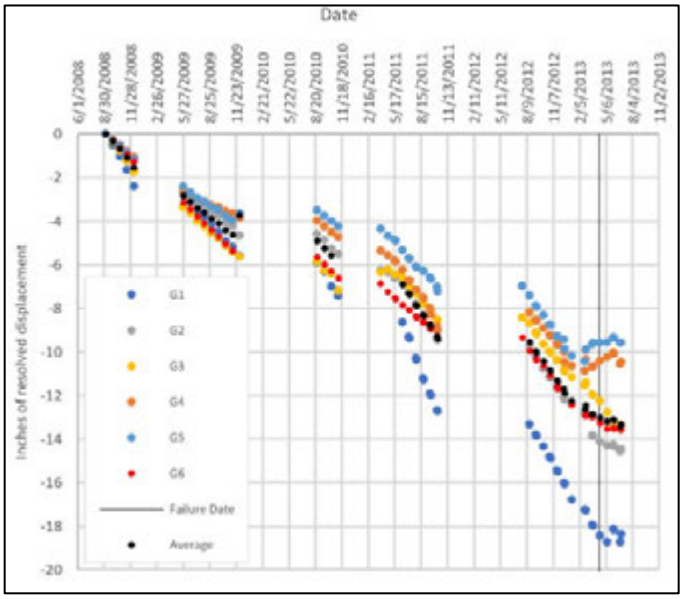

Figure 20: Time series of deformation inside the failure mass for groups G1 to G6.

The areas below the passive block (areas G7 and G8) also show progressive trends up to the time of failure. It is suggested that the deformation of these areas reduced the resistance of the passive block, contributing to the destabilization of the larger mass.

Area G10 is a known stable slope area. Figure 21 shows the stark difference in deformation trend for this zone compared with those within the failure area (areas G1 - G6).

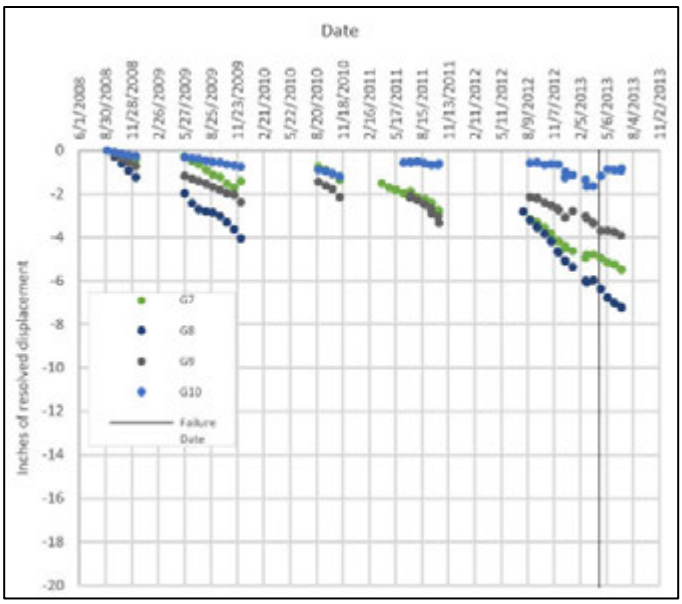

Figure 21: Time series of deformation within (areas G1 to G6) versus outside (area G10) the failure mass

7.3. *Direction of the Movement*

Where and when both the ascending and descending InSAR images are available, it is possible to resolve a movement vector in the plane of the two satellites (east–west and up-down plane). Figures 22 and 23 show the line of sight movements from the descending and ascending orbits respectively.

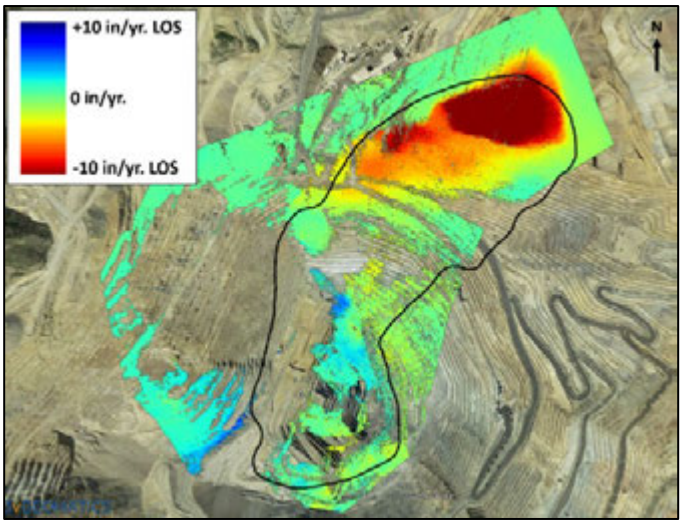

Figure 22: Plan view of Manefay Failure, with line of sight InSAR data, 2011 to 2012, descending satellite.

Figure 24 shows the resolved movement directions. Analysis indicates that the hotspot on the upper failure margin has a dominant downward component, with the remainder of the failure area, lower block, showing a predominantly westerly component. This deformation broadly supports the active/passive wedge failure mechanism hypothesis with the upper block having dropped down, similar to formation of a graben in an extensional tectonic environment.

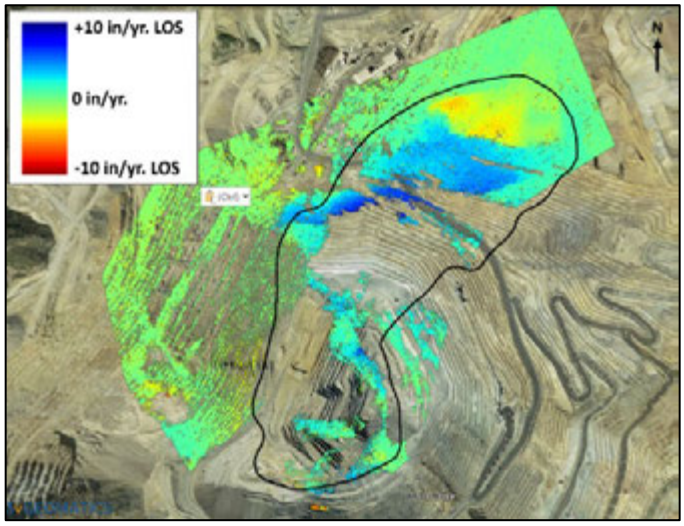

Figure 23: Plan view of Manefay Failure, with line of sight InSAR data, 2011 to 2012, ascending satellite.

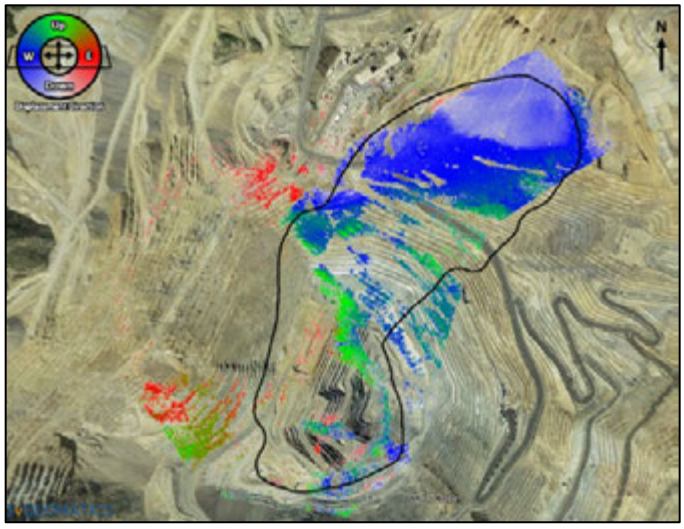

Figure 24: Plan view of the Manefay Failure, shows resolved 2D (east-west and up-down) deformation directions.

7.4. *Failure extents compared to InSAR Data*

Given that InSAR imagery provides a broad, aerial perspective of the Manefay failure it can be used to view all slope aspects. In Figure 25, the combined InSAR data for the period 2008 to 2013 is compared to a satellite photo of the failure. This clearly demonstrates that, in hindsight, assessment of the pre-failure InSAR data could have better predicted the extents of Manefay deformations.

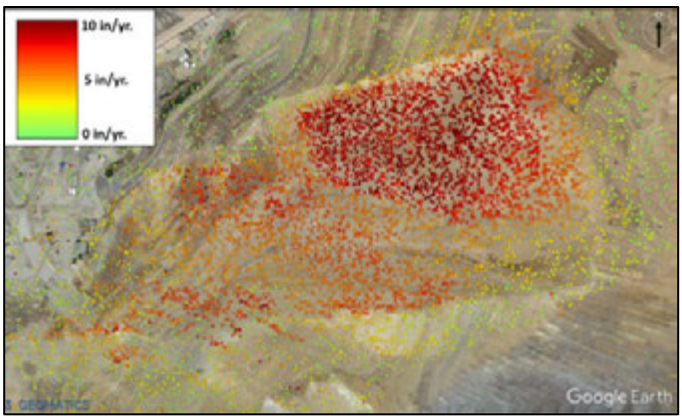

Figure 25: InSAR data points, and average movement rate from 2008 to 2013, relative to satellite image of the failure area. Maximum rate of 10 in/yr.

8. CONCLUSIONS

The Manefay landslide at the Bingham Canyon Mine is arguably the world's largest ever in-pit slope failure. As with any significant geotechnical event, it is important to understand it in order to learn and prevent similar occurrences in the future.

Analytical methods for processing InSAR data have improved significantly since the time leading up to the Manefay failure. Use of these updated methods has indicated that significant ground movements were occurring over a number of years prior to failure. Detailed knowledge of these movements could potentially have led to a different interpretation of failure mechanisms and magnitude. In hindsight, this improved knowledge could have led to adoption of different slope management and mine development plans in the years preceding slope failure. This could have included different mine sequencing and/or advance unloading of the upper Manefay slope.

From a business and operations perspective, the ability to identify these "weak signals" prior to catastrophic slope deformations is essential to appropriate management of such events.

The use of InSAR, as discussed in this paper, provides an increased capability for further improved slope management at RTKC, and at other mining operations.

9. ACKNOWLEDGEMENTS

The authors would like to thank Rio Tinto, and in particular the Bingham Canyon Mine, for allowing this information to be published and shared.

10. REFERENCES

1. Eberhardt, E., D. Stead, T. Styles, and W. Kyusek. 2010. Integration of InSAR with Advanced Numerical Modeling Methodology & Results, Mine Subsidence Monitoring (MSM) EOADP Project. *Report delivered to RTKC, Report # MSM-UBCSFU-10-004*

2. Gibbs, J. 2018. Bingham Canyon Geology Map. *Rio Tinto Internal Report*

3. Gibbs, J. 2019. Manefay Cross-section. *Rio Tinto Internal Report*

4. Heiner, J. 2014. Plot of Runout Prediction vs Actual. *Rio Tinto Internal Report*

5. Moffitt K., D, Cambio, J. Carvalho, M. Gaida, J. Jung, M. Yetisir, and T. Sherizadeh. 2018. Back-Analysis of the Bingham Canyon South Wall: A Quasi-Static Complex Movement Mechanism. *ARMA 18-1366*

6. Pankow, K.L., J.R Moore, M. Hale, K.D. Koper, K.M. Whidden and M.K. McCarter. 2013. Massive landslide at Utah copper mine generates wealth of geophysical data. *GSA Today, Volume 24, Issue 1, pp. 4-9*

7. Porter J., K. Schroeder, and G. Austin. 2012. Geology of Bingham Canyon Porphyry Cu-Mo-Au Deposit. *Society of Economic Geologists Special Publication 16, pp.127 -146*

8. Presnell, R.D. 1998. Structural Controls on the Plutonism and Metallogeny in the Wasatch and Oquirrh Mountains, Utah. *Society of Economic Geologists Guidebook Series, Volume 29*

9. Ross B. 2016. Rise to the Occasion, Lessons from the Bingham Canyon Manefay Slide, *Society for Mining, Metallurgy, & Exploration Inc. (SME), ISBN 978-0-87335-431-8, Ebook 978-0-87335-434-9.*